

NPS ARCHIVE
1959
NAMIKAWA, Y.

MOTION OF THE TROPICAL STORM

YOSHITAKA NAMIKAWA

Released by Committee 11/20/68.

Y
ALFRED W. WHITE SCHOOL
MILWAUKEE, WISCONSIN

MOTION OF THE TROPICAL STORM

* * * * *

Yoshitaka Namikawa

MOTION OF THE TROPICAL STORM

by

Yoshitaka Namikawa

Lieutenant, Japanese Maritime

Self Defense Force

Submitted in partial fulfillment of
the requirements for the degree of

MASTER OF SCIENCE
IN
METECROLOGY

United States Naval Postgraduate School
Monterey, California

1 9 5 9

NPS ARCHIVE

1959

NAMIKAWA, Y.

~~Thesis~~

MOTION OF THE TROPICAL STORM

by

Yoshitaka Namikawa

This work is accepted as fulfilling
the thesis requirements for the degree of

MASTER OF SCIENCE

IN

METEOROLOGY

from the

United States Naval Postgraduate School

ABSTRACT

Equations for the motion of a tropical storm are derived by assuming that the wind field consists of the vortex motion superimposed on a basic current.

The differential equations are integrated numerically for a variety of typical pressure fields, namely, a constant pressure gradient representing straight parallel isobars; a high pressure cell, represented by an elliptical paraboloid; and a "col", represented by a hyperbolic paraboloid.

The writer wishes to express his appreciation for the assistance and encouragement given him in this investigation by Professor G. J. Haltiner of the U. S. Naval Postgraduate School.

TABLE OF CONTENTS

Section	Title	Page
1	Introduction	1
2	Development of the Equation of Motion	3
3	Computations and Solutions	10
4	Verification	21
5	Conclusions	28
6	Bibliography	29

LIST OF ILLUSTRATIONS

Figure		Page
1.	Illustration for Blaton's formula	4
2.	Illustration for the Coriolis parameter as a function of the latitude.	6
3.	Illustration for the tropical vortex	7
4.	Illustration for sign of the cardinal direction	9
5.	A representation of a high pressure cell by an elliptical paraboloid	11
6.	A representation of a "ccl" by a hyperbolic paraboloid	12
7.	Paths of a vortex for several orientations of straight parallel isobars	14
8.	Paths of a vortex for several initial velocities and basic pressure gradients in the case of straight parallel isobars	15
9.	The paths of a vortex as a function of the initial latitude	16
10.	Paths of a vortex for varying vortex size and intensity	17
11.	The path of a vortex for an elliptic basic pressure pattern	18
12.	Paths of a vortex for a hyperbolic basic pressure pattern	20
13.	The first computation for typhoon "Clara" of Nov. 1950, I	22
14.	The second computation for typhoon "Clara" of Nov. 1950, II	24
15.	The third computation for typhoon "Clara" of Nov. 1950, III	25
16.	A computation for typhoon "Jean" of Oct. 1956	27

Table	Page
I The data for Figure 7	13
II The data for Figure 8	15
III The data for Figure 9	16
IV The data for Figure 10	17
V The data for Figure 11	18
VI The data for Figure 12	19
VII The data for Figure 13	21
VIII The data for Figure 16	26

1. INTRODUCTION.

Many methods for the prognosis of the motion of tropical storms have been attempted. They may be divided into two main classes.

The first method is based on kinematical considerations and the use of the pressure tendency as developed by Elliott [2] and Petterssen [6]. Murakami, Masuda and Arakawa [5] adapted this technique to quantitative prediction.

The second method is based on dynamical considerations which consider the tropical storm as the vortex in the atmosphere. Yeh [9] analyzed the external and internal forces acting on Rankine model vortex, based on the Blasius law by using complex potential. As the solution of his equation, he found the circular path without the basic motion, and the trochoidal path with the basic motion which has uniform velocity. Kuo [4], Takeuchi [8] analyzed the forces by using a stream function for the basic flow which has constant vorticity. Kasahara [3] developed the idea of stream function for numerical prediction based on the barotropic model. Syono [7] derived the equation of motion for the vortex in a non-uniform pressure field from some what more general considerations, and illustrated oscillatory motion of vortex.

The approach in this paper is similar to that of Syono but uses a more complicated model of the vortex. Also, for numerical predicting purposes the variability of the Coriolis factor with latitude is taken into account in the equations.

Because of the difficulties in obtaining analytical

solutions are obtained by the Runge-Kutta-Gill method on a National Cash Register 102A electronic computer. A half-hour time increment is sufficient to integrate the equations for this purpose. About 40 minutes are needed to compute a 24 hour path. Moreover three typical basic pressure fields are utilized in this paper, namely straight isobars, an elliptical high pressure cell, and a col. These pressure systems are represented mathematically by the following quadratic surfaces; a plane, an elliptic paraboloid and a hyperbolic paraboloid. The last one is an especially interesting case because it relates to the recurvature of the tropical storm.

The application of these solutions for numerical prediction is not covered completely in this paper. However by taking the variability of basic pressure field, size and intensity of storm as a function of time and space, the method shows promise of fair accuracy.

2. Development of the equation of motion

Neglecting the vertical motion, friction force and earth's curvature, and taking a cartesian coordinate system with x and y positive eastward and northward, U and V are x and y components of velocity and the equations of motion for a air particle on the rotating earth are

$$\begin{aligned}\frac{dU}{dt} &= -\frac{1}{\rho} \frac{\partial P}{\partial x} + f V \\ \frac{dV}{dt} &= -\frac{1}{\rho} \frac{\partial P}{\partial y} - f U\end{aligned}\tag{1}$$

where

$$f = 2 \Omega \sin \phi$$

ϕ ; the latitude

Ω ; the angular velocity of rotating earth

ρ ; the density of air

P ; the atmospheric pressure

We shall separate this motion into the basic and rotating motion. Assuming air density is uniform everywhere,

$$\begin{aligned}\text{let } P &= p + p' \\ U &= u + u' \\ V &= v + v'\end{aligned}\tag{2}$$

where P, U, V represent the total motion; p, u, v , the basic; and p', u', v' , the rotating motion.

Substituting (2) into (1) we obtain

$$\begin{aligned}\frac{dU}{dt} &= -\frac{1}{\rho} \frac{\partial p}{\partial x} - \frac{1}{\rho} \frac{\partial p'}{\partial x} + f v + f v' \\ \frac{dV}{dt} &= -\frac{1}{\rho} \frac{\partial p}{\partial y} - \frac{1}{\rho} \frac{\partial p'}{\partial y} - f u - f u'\end{aligned}\tag{3}$$

We shall assume now that the rotating circular vortex moves without deformation and that the gradient wind approximation may be taken to represent the pressure contribution of the vortex as follows

$$\frac{1}{\rho} \frac{\partial p}{\partial r} = \frac{v_t^2}{r_t} + f v_t \quad (4)$$

where v_t is the tangential velocity and r_t is radius of the particle trajectory.

Blaton's formula states

$$r_t = r_s \left(1 - \frac{c}{v_t} \cos \psi\right)^{-1} \quad (5)$$

Here r_s is radius of streamline, and c is velocity of system, and ψ is angle between c and v_t .

From Fig. 1

$$\psi = \left(\frac{\pi}{2} + \theta\right) - \theta_t = \frac{\pi}{2} - (\theta_t - \theta)$$

thus

$$\cos \psi = \sin \theta_t \cos \theta - \cos \theta_t \sin \theta \quad (6)$$

and

$$c \sin \theta_t = C_y \quad (7)$$

$$c \cos \theta_t = C_x$$

Combining (5), (6) and (7) leads to

$$r_t = r_s \left[1 - \frac{1}{v_t} (C_y \cos \theta - C_x \sin \theta)\right]^{-1} \quad (8)$$

No simple mathematical

function has been found to represent the wind distribution in the entire tropical storm.

Syono, Yeh, and others have

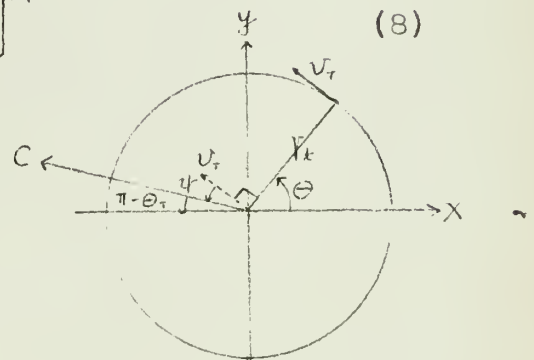


Fig 1

used a Rankine vortex with velocity distribution, $\frac{v_r}{r} = \text{constant}$, for the whole area of the storm. Takahashi introduced the empirical formulas

$$\begin{aligned} v_r r &= \text{constant at the outside of storm} \\ v_r r^{\frac{1}{2}} &= \text{constant in the outer region} \\ &\quad (\text{about within } r = 500 \text{ kms}) \\ v_r r^{-1} &= \text{constant in the inner region} \\ &\quad (\text{about within } r = 40 \text{ kms}) \end{aligned}$$

In this paper, the Rankine model will be taken for inner region and a hyperbolic wind distribution for outer region, following [1], namely:

$$v_r = \omega r \quad ; \quad 0 \leq r \leq a \quad (9)$$

$$v_r = \frac{K}{r} \quad ; \quad a \leq r \leq r_1 \quad (9')$$

ω is the angular velocity of rotating vortex, K is constant, a and r_1 are the radii of the inner region and outer boundaries, respectively.

From (4)

$$\frac{1}{r} \frac{\partial p'}{\partial x} = \cos \theta \cdot \frac{1}{r} \frac{\partial p'}{\partial r} = \cos \theta \cdot v_r \left(\frac{v_r}{r^2} + f \right)$$

$$\frac{1}{r} \frac{\partial p'}{\partial y} = \sin \theta \cdot \frac{1}{r} \frac{\partial p'}{\partial r} = \sin \theta \cdot v_r \left(\frac{v_r}{r^2} + f \right)$$

Substituting (8), (9), (9') into the above equations

$$-\frac{1}{r} \frac{\partial p'}{\partial x} = -\cos \theta \cdot \omega^2 r_s + \omega (C_y \cos^2 \theta - C_x \sin \theta \cdot \cos \theta) - \cos \theta \omega r_s f \quad (10)$$

$$; \quad 0 \leq r \leq a$$

$$\text{and} \quad = -\cos \theta \cdot \frac{K^2}{r_s^2} + \frac{K}{r_s^2} (C_y \cos^2 \theta - C_x \sin \theta \cdot \cos \theta) - \cos \theta \cdot \frac{K f}{r_s} \quad (10')$$

$$; \quad a \leq r \leq r_1$$

$$-\frac{1}{r} \frac{\partial p'}{\partial y} = -\sin \theta \cdot \omega^2 r_s + \omega (C_y \cos \theta \cdot \sin \theta - C_x \sin^2 \theta) - \sin \theta \omega r_s f \quad (11)$$

$$\text{and} \quad = -\sin \theta \cdot \frac{K^2}{r_s^2} + \frac{K}{r_s^2} (C_y \cos \theta \cdot \sin \theta - C_x \sin^2 \theta) - \sin \theta \cdot \frac{K f}{r_s} \quad (11')$$

$$; \quad a \leq r \leq r_1$$

Later, r will be used instead of r_s .

Now $f = 2\Omega \sin\phi$ is a Coriolis parameter and is a function of the latitude. Let the latitude at center of vortex be ϕ_s , and R, r the radii of earth and vortex, respectively

The latitude at any point in the vortex r, θ as measured from the vortex center may be represented as follows:

$$\phi = \phi_s + d\phi = \phi_s + \frac{r \sin\theta}{R}, \quad \sin\phi = \sin\left(\phi_s + \frac{r \sin\theta}{R}\right)$$

as shown in Fig. 1 and Fig. 2.

Expanding $\cos \frac{r \sin\theta}{R}$ and $\sin \frac{r \sin\theta}{R}$ in series form and neglecting terms of higher order than the second gives

$$\begin{aligned} \sin\phi &= \sin\phi_s \cos\left(\frac{r \sin\theta}{R}\right) + \cos\phi_s \sin\left(\frac{r \sin\theta}{R}\right) \\ &\approx \sin\phi_s \left(1 - \frac{r^2 \sin^2\theta}{2R^2}\right) + \cos\phi_s \cdot \left(\frac{r \sin\theta}{R}\right) \end{aligned} \quad (12)$$

Next integrating equation (3) over the whole area of vortex, which is shown in Fig 3, we obtain

$$\begin{aligned} \frac{1}{s} \oint \frac{d\bar{\pi}}{dt} ds &= -\frac{1}{s} \oint \frac{1}{\rho} \frac{\partial p}{\partial x} ds - \frac{1}{s} \oint \frac{1}{\rho} \frac{\partial p'}{\partial x} ds + \frac{1}{s} \oint f v ds + \frac{1}{s} \oint f' v' ds \\ \frac{1}{s} \oint \frac{d\bar{v}}{dt} ds &= -\frac{1}{s} \oint \frac{1}{\rho} \frac{\partial p}{\partial y} ds - \frac{1}{s} \oint \frac{1}{\rho} \frac{\partial p'}{\partial y} ds - \frac{1}{s} \oint f u ds - \frac{1}{s} \oint f' u' ds \end{aligned} \quad (13)$$

Now, let

$$-\frac{1}{\rho} \frac{\partial p}{\partial x} = b_x, \quad -\frac{1}{\rho} \frac{\partial p'}{\partial y} = b_y$$

$$C_x = \frac{1}{s} \oint \bar{\pi} ds = \frac{1}{s} \oint u ds$$

$$C_y = \frac{1}{s} \oint \bar{v} ds = \frac{1}{s} \oint v ds$$

Integrating the first term

on the right side of equation

(13) yields

$$\oint b_x ds = \pi r_1^2 \bar{b}_x$$

$$\oint b_y ds = \pi r_1^2 \bar{b}_y$$

where \bar{b}_x, \bar{b}_y , are mean values.

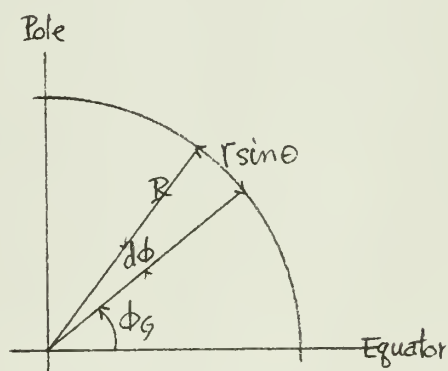


Fig 2.

Furthermore, by use of equations (10) and (11)

$$\begin{aligned} -\oint \frac{1}{r} \frac{\partial p'}{\partial x} ds &= \int_0^{2\pi} \int_0^a \left\{ -\cos\theta \cdot \omega^2 r + \omega (C_y \cos^2\theta - C_x \sin^2\theta \cdot \cos\theta) \right\} ds \\ &\quad + \int_0^{2\pi} \int_a^{r_1} \left\{ -\cos\theta \cdot \frac{K^2}{r^3} + \frac{K}{r^2} (C_y \cos^2\theta - C_x \sin^2\theta \cdot \cos\theta) \right\} ds - \oint \cos\theta f u_r ds \\ &= \frac{\omega}{2} a^2 C_y \cdot \pi + K \ln \frac{r_1}{a} \cdot C_y \cdot \pi - \oint f u_r ds \end{aligned}$$

$$\begin{aligned} -\oint \frac{1}{r} \frac{\partial p'}{\partial y} ds &= \int_0^{2\pi} \int_0^a \left\{ -\sin\theta \cdot \omega^2 r + \omega (C_y \cos\theta \cdot \sin\theta - C_x \sin^2\theta) \right\} ds \\ &\quad + \int_0^{2\pi} \int_a^{r_1} \left\{ -\sin\theta \cdot \frac{K^2}{r^3} + \frac{K}{r^2} (C_y \cos\theta \cdot \sin\theta - C_x \sin^2\theta) \right\} ds - \oint \sin\theta f u_r ds \\ &= -\frac{\omega}{2} a^2 C_x \cdot \pi - K \ln \frac{r_1}{a} \cdot C_x \pi + \oint f u_r ds \end{aligned}$$

$$\oint f u_r ds = C_y \cdot 2\Omega \sin\phi_g \cdot S$$

$$-\oint f u_r ds = -C_x \cdot 2\Omega \sin\phi_g \cdot S.$$

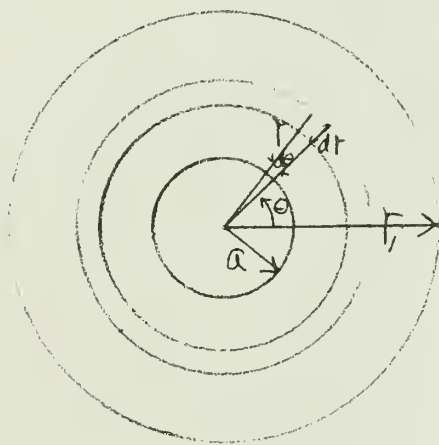


Fig 3

Therefore the equations of motion become

$$\begin{aligned} \frac{dC_x}{dt} &= 2\Omega \sin\phi_g \cdot C_y + \bar{b}_x + \frac{a^2}{2r_1^2} \omega \cdot C_y + \frac{K}{r_1^2} \ln \frac{r_1}{a} \cdot C_y \\ \frac{dC_y}{dt} &= -2\Omega \sin\phi_g \cdot C_x + \bar{b}_y - \frac{a^2}{2r_1^2} \omega \cdot C_x - \frac{K}{r_1^2} \ln \frac{r_1}{a} \cdot C_x \end{aligned} \quad (14)$$

Since ϕ_g is a function of y ,

$$\begin{aligned}\sin \phi_g &= \sin \phi_0 + y \frac{\cos \phi_0}{R} + \dots \dots \dots \\ 2\Omega \sin \phi_g \cdot C_y &\doteq 2\Omega \sin \phi_0 \cdot C_y + 2\Omega \cos \phi_0 \cdot \frac{y}{R} C_y \\ -2\Omega \sin \phi_g \cdot C_x &\doteq -2\Omega \sin \phi_0 \cdot C_x - 2\Omega \cos \phi_0 \cdot \frac{y}{R} C_x\end{aligned}\quad (15)$$

where ϕ_0 corresponds to $y = 0$. Changes in the angular velocity of the vortex may be approximated by assuming the conservation of absolute vorticity of the vortex after Syono [7].

$$\begin{aligned}\omega &= \omega_0 + \Omega (\sin \phi_0 - \sin \phi) \\ \sin \phi &\doteq \sin \phi_0 (1 - \frac{1}{2} \frac{y^2}{R^2}) + \cos \phi_0 (\frac{y}{R})\end{aligned}\quad (16)$$

Therefore

$$\begin{aligned}\frac{a^2}{2r_1^2} \omega C_y &\doteq \frac{\omega_0}{2r_1^2} a^2 C_y + \frac{\Omega a^2}{4r_1^2 R^2} C_y y^2 \sin \phi_0 - \frac{\Omega a^2}{2r_1^2 R} C_y \cos \phi_0 y \\ -\frac{a^2}{2r_1^2} \omega C_x &\doteq -\frac{\omega_0}{2r_1^2} a^2 C_x - \frac{\Omega a^2}{4r_1^2 R^2} C_x y^2 \sin \phi_0 + \frac{\Omega a^2}{2r_1^2 R} C_x \cos \phi_0 y\end{aligned}$$

Finally, the equations of motion are

$$\begin{aligned}\frac{dC_y}{dt} &= \bar{b}_y + 2\Omega \sin \phi_0 \cdot C_y + \frac{2\Omega \cos \phi_0 y}{R} \cdot C_y + \frac{\omega_0}{2r_1^2} a^2 C_y + \frac{\Omega a^2}{4r_1^2 R^2} C_y y^2 \sin \phi_0 \\ &\quad - \frac{\Omega a^2}{2r_1^2 R} C_y \cos \phi_0 y + \frac{K}{r_1^2} \ln \frac{r_1}{a} \cdot C_y\end{aligned}\quad (17)$$

$$\begin{aligned}\frac{dC_x}{dt} &= \bar{b}_x - 2\Omega \sin \phi_0 \cdot C_x - \frac{2\Omega \cos \phi_0 y}{R} \cdot C_x - \frac{\omega_0}{2r_1^2} a^2 C_x - \frac{\Omega a^2}{4r_1^2 R^2} C_x y^2 \sin \phi_0 \\ &\quad + \frac{\Omega a^2}{2r_1^2 R} C_x \cos \phi_0 y - \frac{K}{r_1^2} \ln \frac{r_1}{a} \cdot C_x\end{aligned}$$

Next we shall check the magnitude of each term in the right side of the equation (17). When x, y are taken as 1000 km, and $c_x = c_y = 5$ Kts, the magnitude of each term is as follows:

(1) $+\frac{a^2}{2r_1^2} \omega_0 C_y, -\frac{a^2}{2r_1^2} \omega_0 C_x$; $10' \sim 10^2$ km hr ⁻²
(2) $+\frac{\Omega a^2}{4R^2 r_1^2} \sin \phi_0 \cdot C_y y^2, -\frac{\Omega a^2}{4R^2 r_1^2} \sin \phi_0 \cdot C_x y^2$; $10^{-2} \sim 10^{-3}$ km hr ⁻²
(3) $-\frac{\Omega a^2}{2r_1^2 R} \cos \phi_0 \cdot C_y \cdot y, +\frac{\Omega a^2}{2r_1^2 R} \cos \phi_0 \cdot C_x \cdot y$; 10^{-1} km hr ⁻²
(4) $+\frac{K}{r_1^2} \ln \frac{r_1}{a} \cdot C_y, -\frac{K}{r_1^2} \ln \frac{r_1}{a} \cdot C_x$; $10' \sim 10^2$ km hr ⁻²
(5) $+2\Omega C_y \cdot \sin \phi_0, -2\Omega C_x \cdot \sin \phi_0$; $10' \sim 10^2$ km hr ⁻²
(6) $+\frac{2\Omega \cos \phi_0 y}{R} \cdot C_y, -\frac{2\Omega \cos \phi_0 y}{R} \cdot C_x$; $10^{-2} \sim 10^{-3}$ km hr ⁻²

The terms \bar{b}_x , \bar{b}_y are due to basic pressure field, and represent a contribution to the external steering. Terms (5) and (6) provide the Coriolis force for moving vortex. The other terms are due to internal character of the vortex itself. When c_y has positive sign and the vortex has a northward component, terms (1), (2), (4) act toward east, but the term (3) acts westward. The term (3) is relatively small compared with the terms (1), (4), hence the acceleration of the vortex is eastward. In the case of negative c_y , the opposite effects take place. Similarly when c_x has positive sign and vortex is moving eastward, the terms (1), (2), (4) act southward, while the small term (3) acts northward. The result is a net force southward. In the case of negative c_x , the vortex tends to move northward. Comparison of terms (2) and (3), which are functions of y , shows that term (3) dominates term (2). Therefore, a northward movement with an increasing value of y will tend to make term (3) significant. When term (3) becomes sufficiently large, the northward movement tends to increase with positive c_x . Also, the eastward movement decreases or westward movement increases with positive c_y . All directions are considered in the Northern Hemisphere. (Fig 4)

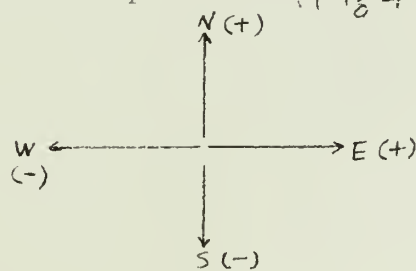


Fig 4

3. Computation and Solutions

The numerical solution is obtained by the digital computer using the Runge-Kutta-Gill method which involves four iterations for each forward step. Half-hour time increments were found to be sufficient for computing the motion of tropical storms from this system of equations. About 40 minutes are needed for computing the 24 hour path on the CRC 102A digital computer at the U. S. Naval Postgraduate School.

Solutions are provided for a variety of conditions, which may be roughly divided into three cases, according to the following basic pressure patterns:

(A) A constant pressure gradient representing straight parallel isobars.

The terms \bar{b}_x , \bar{b}_y in the equation (17) are constant everywhere. Therefore \bar{b}_x , \bar{b}_y represent average values over the area of the vortex.

(B) A high pressure cell, represented by an elliptical paraboloid.

A pressure surface in the vicinity of the subtropical high cell may be approximated by this shape, as shown in Fig. 5, where the coordinates of the center of the high are x_1 , y_1 . Considering the conditions at some pressure level, such as the 700-mb or 500-mb surfaces, the height of the constant pressure surface z is a function of x and y . The equation for the contour height may be written as follows,

$$(z - z_1) = A(x - x_1)^2 + B(y - y_1)^2 \quad (18)$$

where A and B are constants related to the slope of the

pressure surface. Here

$$b_x \zeta = -g \frac{\partial \zeta}{\partial x} = -2gA(x - x_1) \quad (19)$$

$$b_y \zeta = -g \frac{\partial \zeta}{\partial y} = -2gB(y - y_1)$$

The symbol ζ is used for the b_x , b_y at the center of the vortex. If B is small but A is large, equation (18) gives an ellipsoid elongated along x axis. If $A=B$, there is a circular pressure pattern.

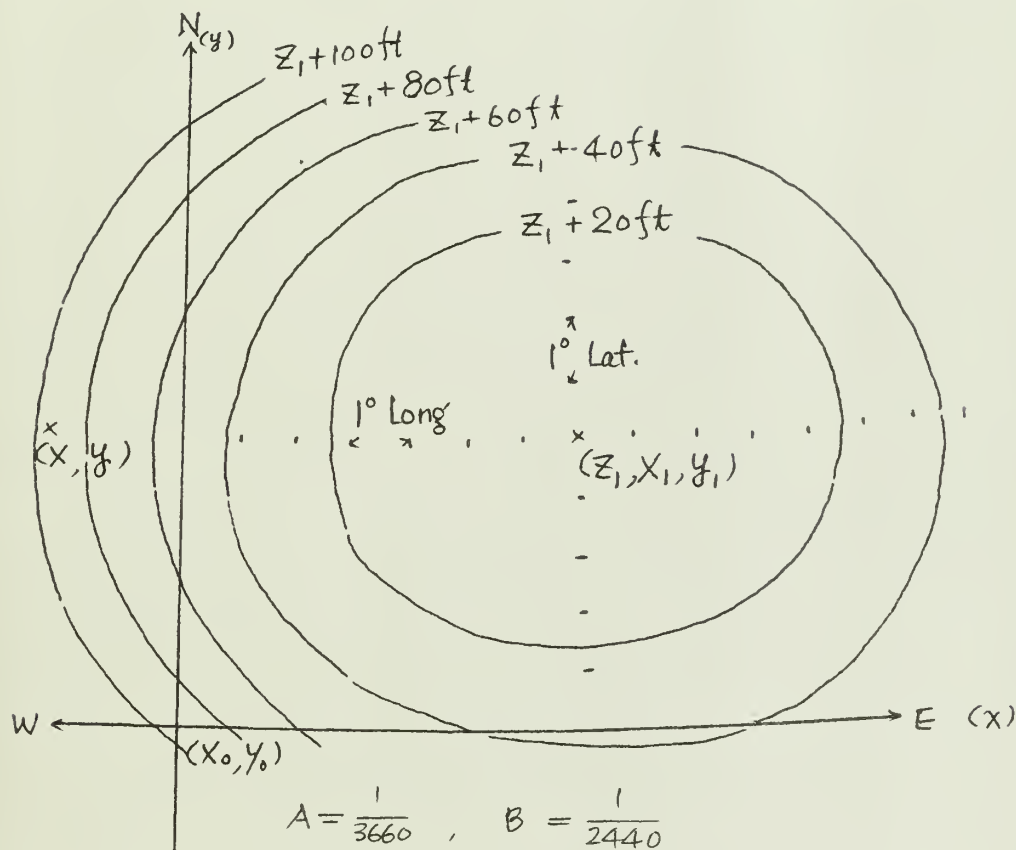


Figure 5

(C) A "col", represented by a hyperbolic paraboloid.

This pattern, which is closely associated with the recurrence of tropical storms, is shown in Figure 6.

The equation for this pattern may be written as follows:

$$(Z - Z_1) = A(x - x_1)^2 - B(y - y_1)^2 \quad (20)$$

where A, B are again constant, It follows that

$$b_{xs} = -g \frac{\partial Z}{\partial x} = -2gA(x - x_1) \quad (21)$$

$$b_{ys} = -g \frac{\partial Z}{\partial y} = +2gB(y - y_1)$$

If B is small but A is large, there will be a strong trough.

On the contrary, a small A with large B indicates a weak trough.

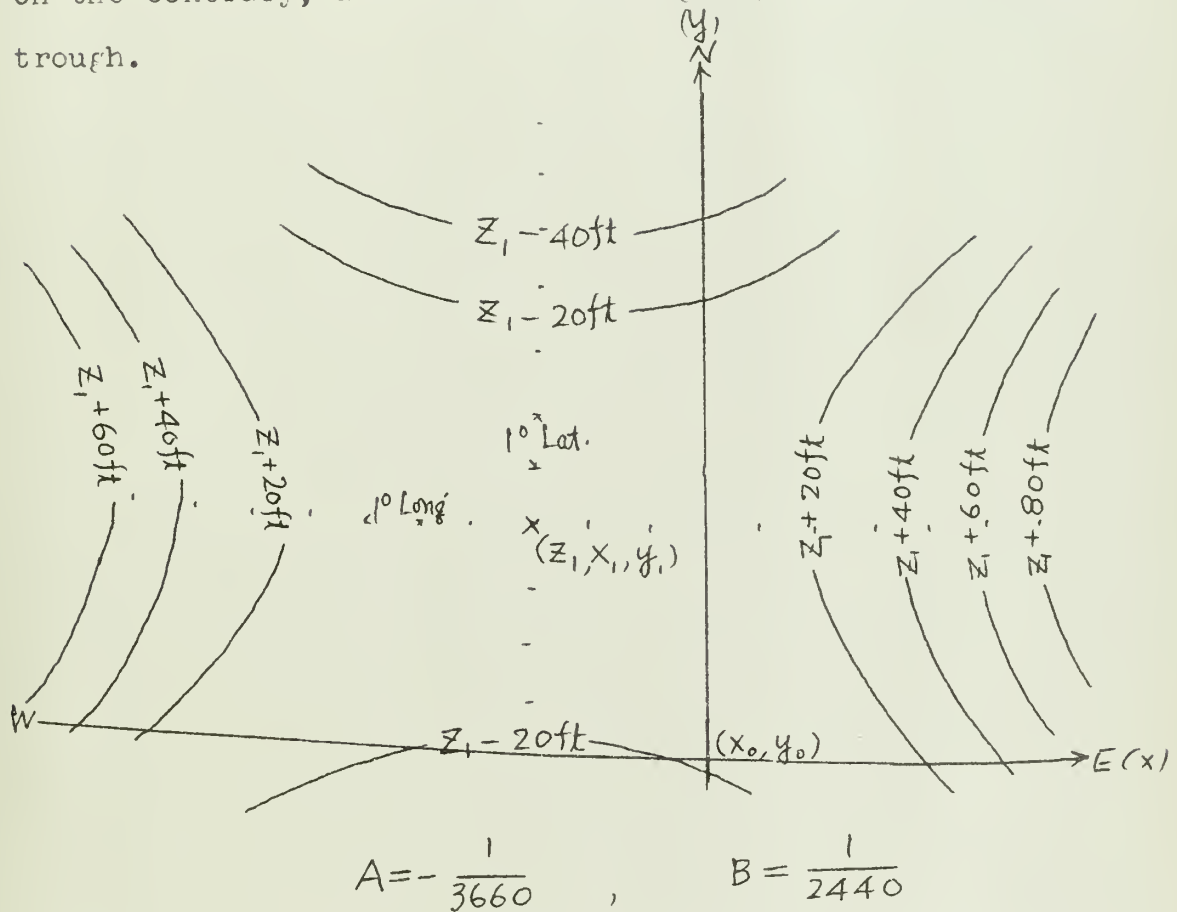


Figure 6

In case (2) and (3) b_x and b_y are not constant.

TABLE I

$\omega = 2 \text{ hr}^{-1}$				$r_1 = 300 \text{ km}$				
$K = 1600 \text{ km}^2 \text{ hr}^{-1}$				$a = 40 \text{ km}$				
$\phi_0 = 15^\circ \text{N}$								
t (hr)	I		II		III		IV	
	C_x	C_y	C_x	C_y	C_x	C_y	C_x	C_y
3	-15.9	+ 9.5	-4.6	+17.2	+ 9.3	+15.9	+17.2	+ 4.1
6	- 6.4	+12.8	+ 5.3	+12.7	+12.8	+ 6.1	+12.8	- 5.1
9	+ 2.8	+ 8.0	+ 8.3	+ 2.3	+ 7.9	- 3.1	+ 3.2	- 8.2
12	+ 5.5	- 1.9	+ 2.9	- 6.1	- 2.3	- 5.6	- 5.6	- 3.2
15	- 0.1	-11.1	- 7.4	- 8.1	-10.9	+ 2.3	- 8.1	+ 6.6
18	-10.2	-12.4	-15.7	- 1.8	-12.4	+10.5	- 2.6	+15.1
21	-18.3	- 6.3	-16.6	+ 2.6	- 5.7	+16.7	+ 7.5	+16.9
24	-19.4	+ 3.7	- 9.4	+17.2	+ 5.1	+13.8	+15.8	+10.4
27	-12.8	+11.5	+ 1.3	+16.0	+12.5	+10.7	+13.5	+ 0.0
30	- 2.6	+11.9	+ 8.3	+ 7.7	+11.1	+ 0.0	+ 9.1	- 7.7
33	+ 4.8	+ 4.7	+ 6.5	- 3.0	+ 1.8	- 6.3	- 1.5	- 7.2
36	+ 4.4	- 5.6	- 2.8	- 8.6	- 8.8	- 2.9	- 8.1	+ 1.0
39	- 3.5	-12.3	-13.1	- 5.3				
42	-13.7	-11.0	-18.0	+ 4.7				
45	-19.8	- 2.8	-12.5	+14.4				
48			- 1.8	+17.1				

Integrating b_x and b_y , given by equations (19) and (21), over the whole area of the vortex yields

$$\oint b_x r dr d\theta = \oint \{ 2gA [(X + r \cos \theta) - x_1] \} r d\theta dr = -2gA(X - x_1) \cdot S$$

$$\oint b_y r dr d\theta = +2gB(y - y_1) \cdot S$$

Figure 7 and Table I show the path of vortex for several orientations of straight parallel isobars representing the basic pressure field. The models are taken with the data in Table 1. Curves I, II, III, IV are based on a basic pressure field corresponding to a 10 kt geostrophic wind, and a 10 kt initial velocity toward the directions of W, NW, N, NE respect-

ively. Each curve represents a cycloid with the same amplitude and period. When the path is sufficiently long, the curves may differ because of the contribution of term (3) in equation (17).

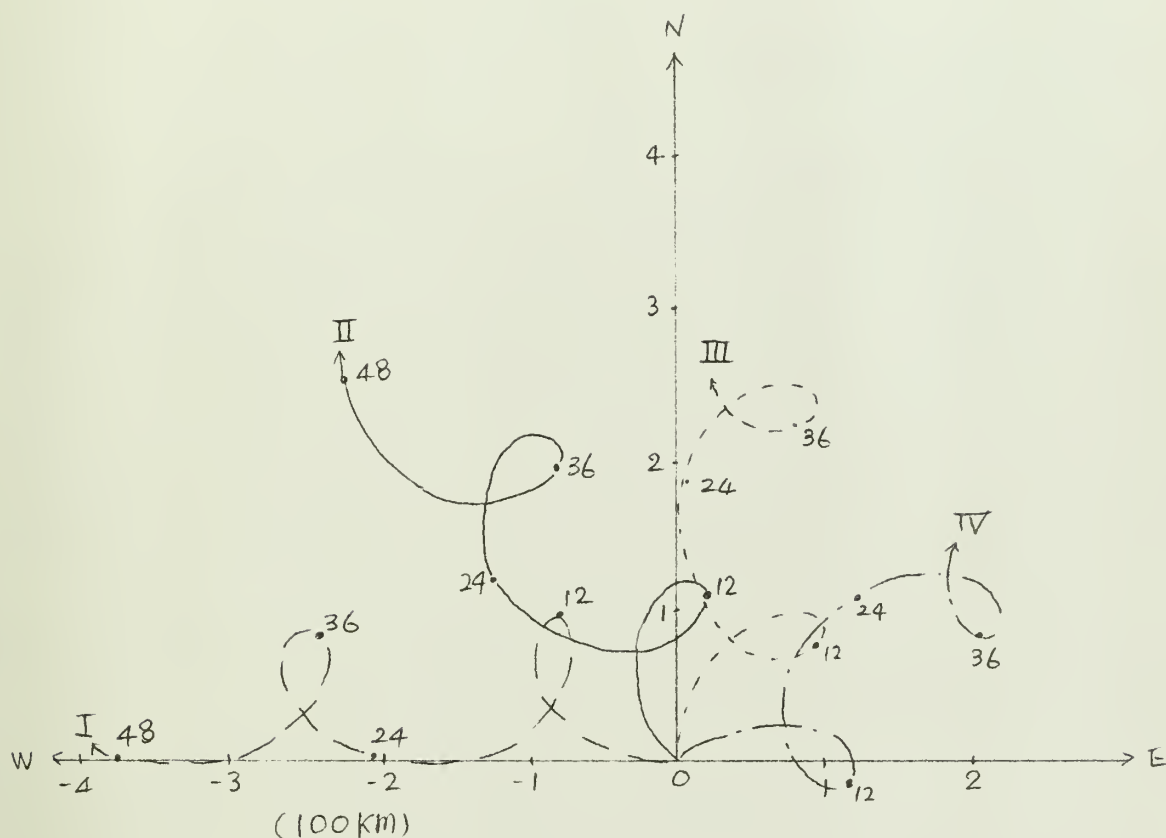


Figure 7

Figure 8 and Table II represent the trajectory for several initial velocities and basic pressure gradients. Other conditions are similar to those in the previous model. Curve I is for zero initial velocity and basic pressure gradient corresponding to a NW 10 kt geostrophic wind. Curve II is for a 5 kt initial velocity and a 5 kt basic geostrophic wind. Curve III is for a 10 kt initial velocity and

basic geostrophic wind. The amplitude increases with increasing initial velocity and with increasing of the magnitude of basic pressure gradient. The period does not change with changing of initial velocity and basic pressure gradient.

TABLE II

		I	II	III
w_0	hr ⁻¹	2	"	"
K	km hr ⁻¹	1600	"	"
Φ_0	° lat. N	15	"	"
L	km	300	"	"
a	km	40	"	"
C_x	direction/kts	0	NW/5	NW/10
C_y	(toward)			
b_x	corresponding	NW/10	NW/5	NW/10
b_y	to V_{gs} .			

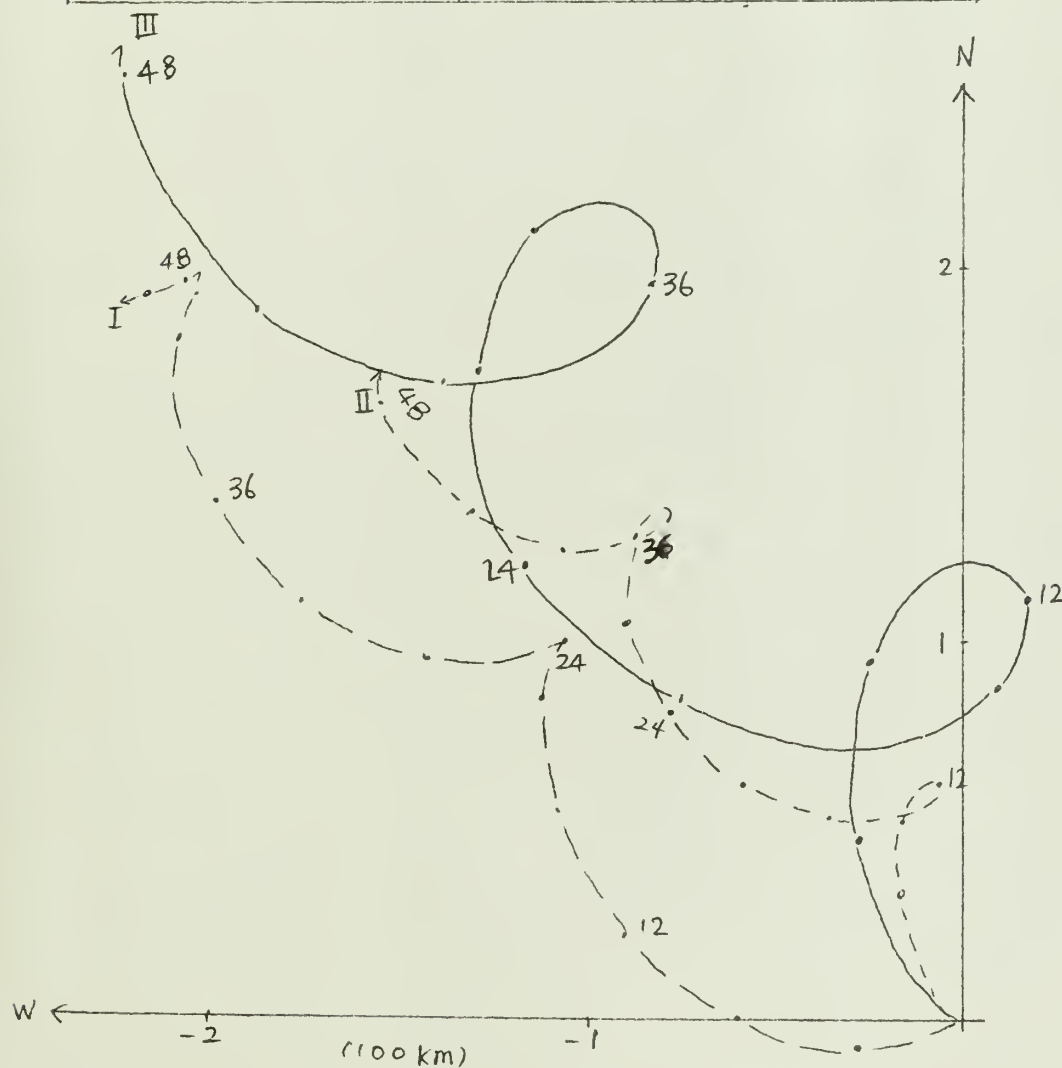


Figure 8

Figure 9 and Table III are for an initial latitude of 25°N , but other data are the same as for the previous case. The results indicate that the amplitude and period decreases with increasing of initial latitude.

TABLE III

ω_0	K	r_1	a	ϕ_0	b	C
2 hr^{-1}	$1600 \text{ km}^2 \text{ hr}^{-1}$	300 km	40 km	25°N	NW/10 kts	NW/10kts

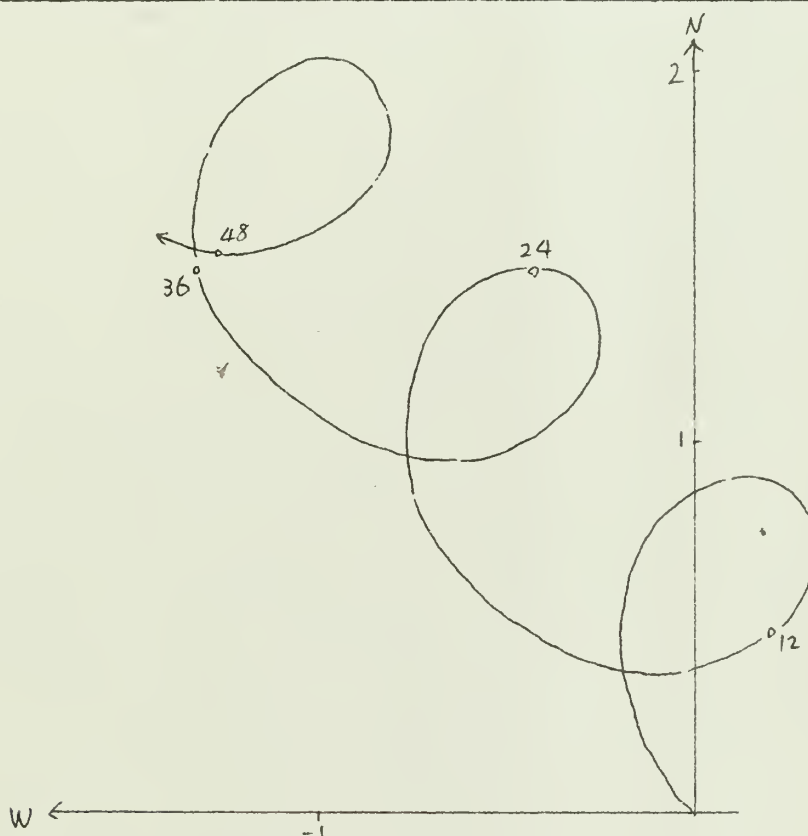


Figure 9

Figure 10 and Table IV represent several cases of different vortex size and intensity. Curve III is same as II in the Figure 7. Curve I is for a case of large angular velocity of the rotating vortex. Curve II represents a large size and strong intensity (large angular velocity). The amplitude and period increase with decreasing intensity and increasing size.

TABLE IV

		I	II	III
ω_0	hr^{-1}	4	"	2
K	$km^2 \cdot hr^{-1}$	6400	"	1600
Φ_0	$^{\circ} \text{Lat } N$	15	"	"
r_1	Km	300	600	300
a	Km	40	"	"
c	direction/Kts	NW/10	"	"
b (v_{gs})	direction/Kts	NW/10	"	"

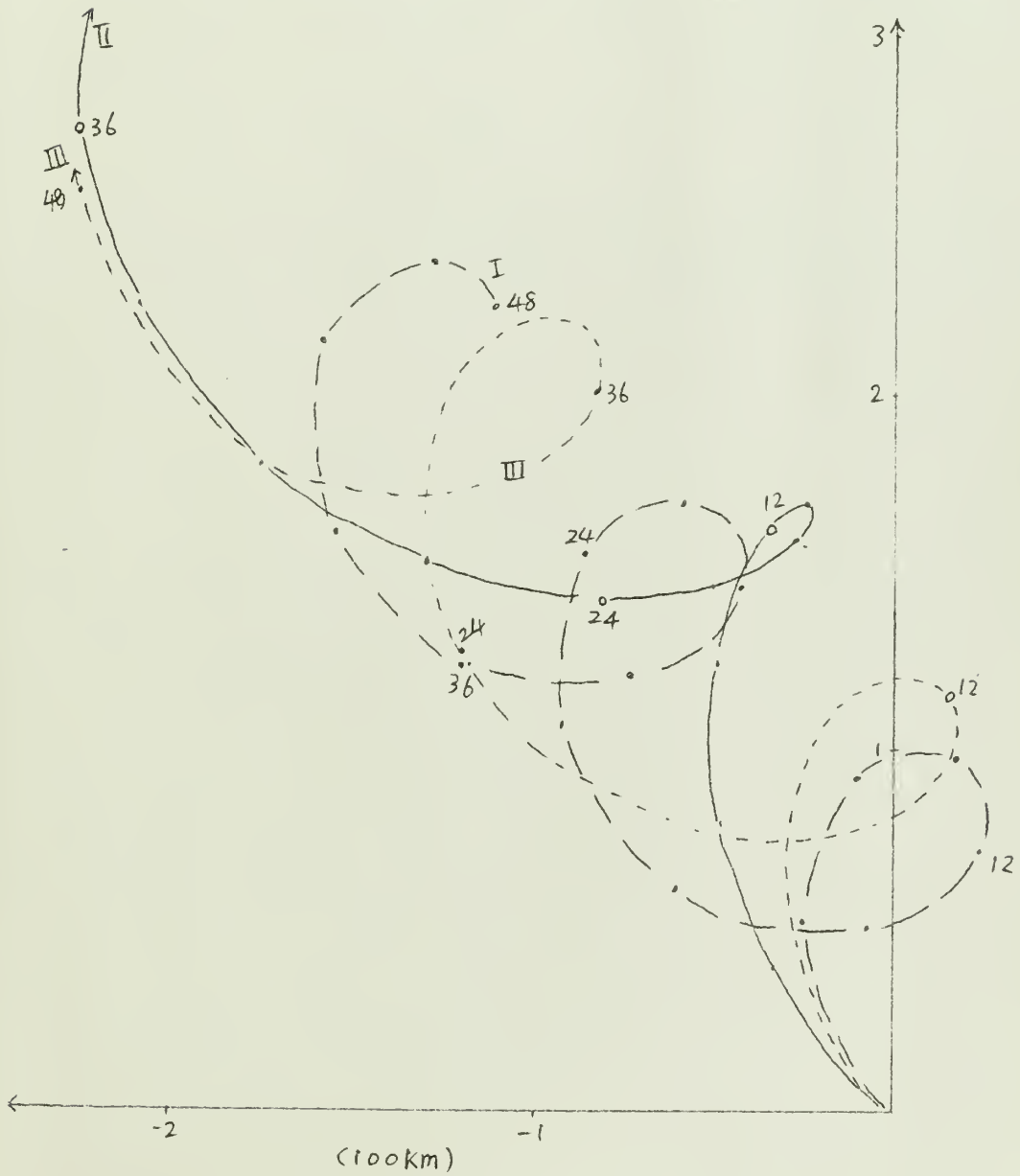


Figure 10

Figure 11 and Table V give the results for an elliptic pressure pattern which has a geostrophic wind velocity of 10 kts at $x = 1110$ kms $y = 0$, and 12.5 kts at $x = 0$, $y = 1110$ kms. The vortex model is taken as same as that of Figure 9. The initial velocity is taken as 80% of basic geostrophic wind. The amplitude increase near the point of recurvature is due to increase of pressure gradient, and so the total speed decreases.

TABLE V

ω_0	K	r_1	a	ϕ_0	x_1	y_1	A	B
4 hr^{-1}	$6400 \text{ km}^2/\text{hr}^2$	600 km	40 km	15°N	0	500 km	$1/320$	$1/5490$

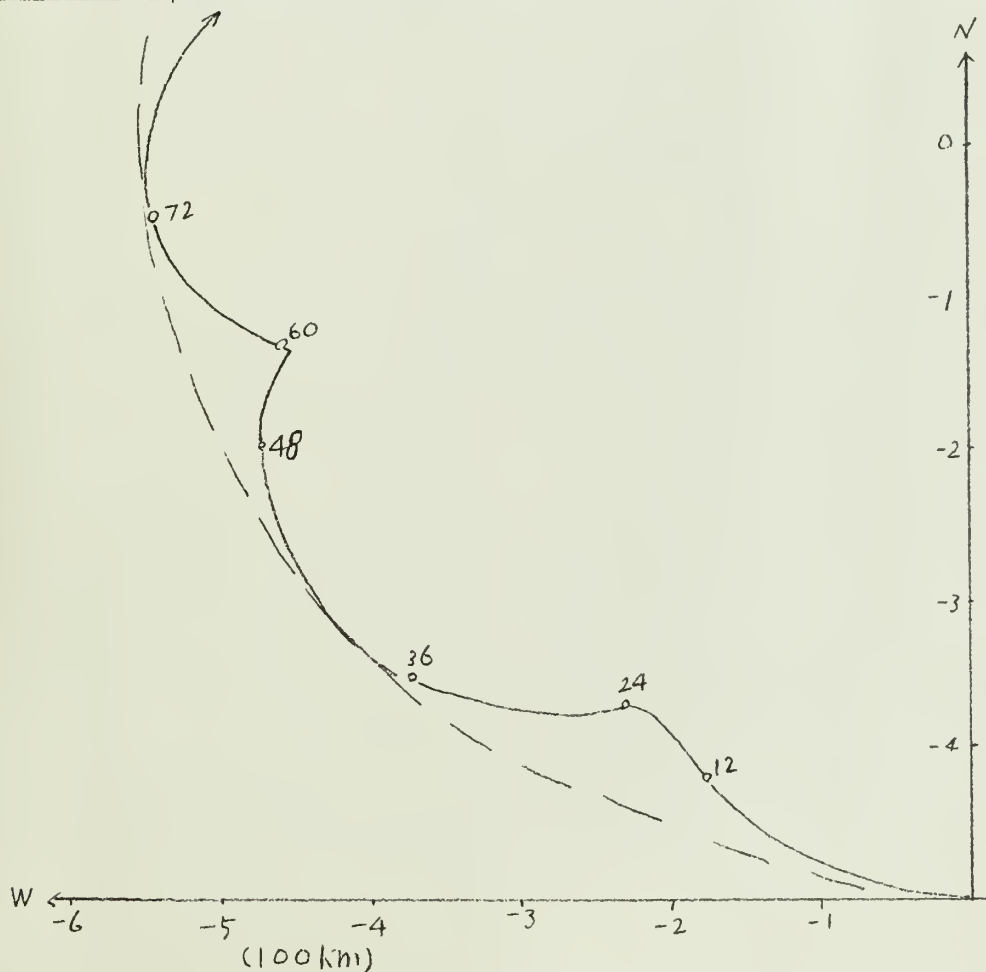


Figure 11

Figure 12 and Table VI are represented for the hyperbolic case. The vortex models are similar to those of Fig. 11, but each track is started from different position as shown in Fig. 12 and Table VI. Tracks I, II recurved toward NE after reaching the latitude where is $y = y_1$, Curves III, IV, V show continuous movement toward the west, together with a tendency southward according to the curvature of the basic isobars. The loop becomes large with crossing to the point of "col". Hence the overall velocity decreases accordingly. Curves II and III result from different starting points which differ by only 50 kms in x direction, but with same y-value. Yet one recurves and other does not. This 50 km distance is a small value compared with the size of the vortex; nevertheless it leads to significantly different results.

TABLE VI

$\omega_0 = 4 \text{ hr}^{-1}$	$A = - \frac{1}{7320}$				
$K = 6400 \text{ km}^2 \text{ hr}^{-1}$	$B = + \frac{1}{5490}$				
$r_1 = 600 \text{ km}$					
$a = 40 \text{ km}$					
$\phi_0 = 15^\circ \text{ N}$					
	I	II	III	IV	V
$x_1 \text{ (km)}$	-800	-400	-350	-300	-200
$y_1 \text{ (km)}$	+400	+400	+400	+400	+400

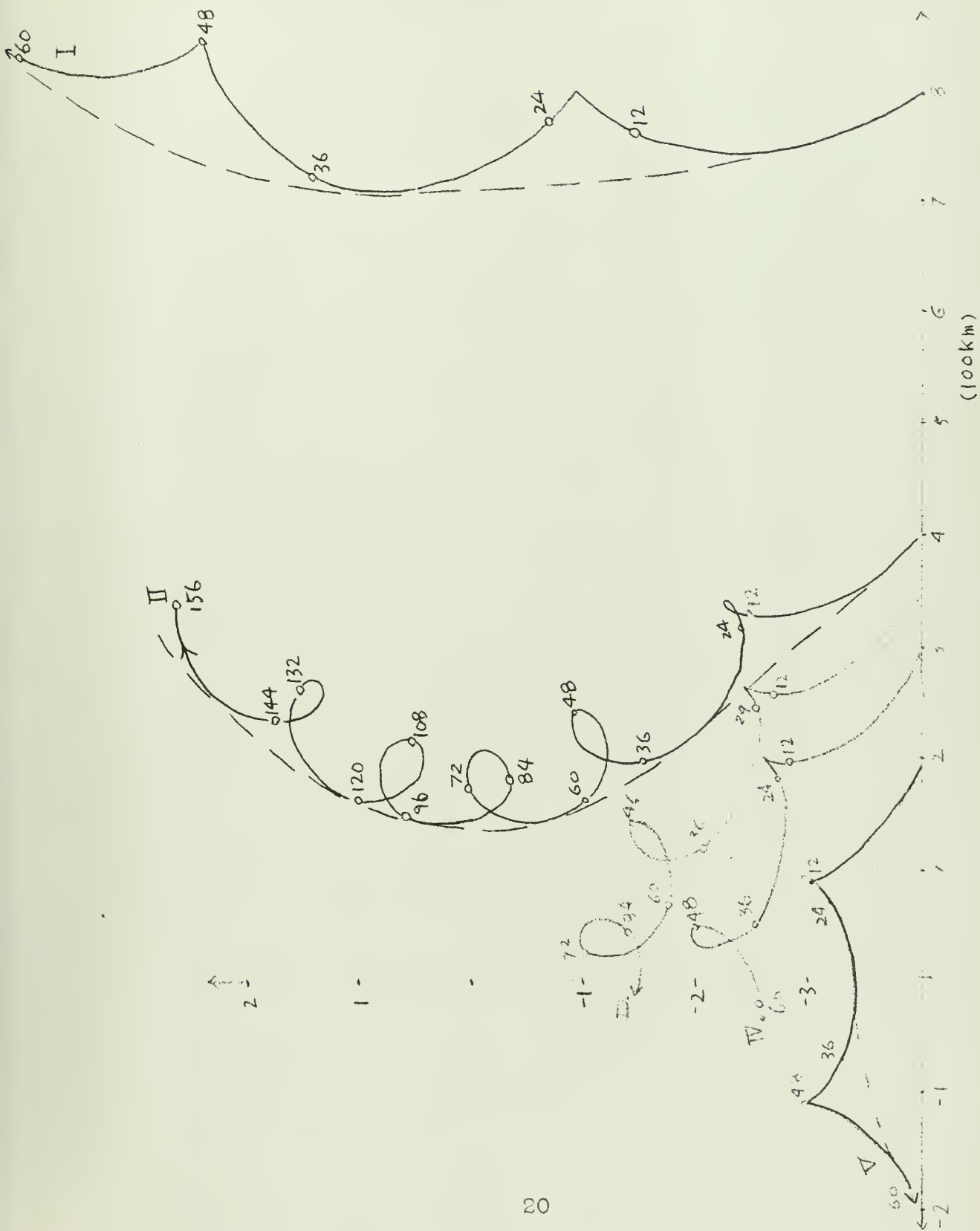


FIGURE 12

4. Verification

Time limitations did not permit adequate testing of the theory, however two actual examples are shown for illustration. The first example is Typhoon "Clara" (Nov. 1950). The starting point is taken on Nov. 7, 1950, 0000 Japanese local time (1500Z 6th), in order to avoid the influence of a second vortex which occurred prior to this time. For prediction purposes, a prognosis of the basic pressure field is needed; however, this type of prognosis is not the subject of this paper. Therefore the time mean map which is the average of the 6th through the 10th will be used instead of a prognostic map. Moreover, the 500-mb pattern will be taken as a basic pressure field. Figure 13 shows this pattern which may be represented by an elliptic paraboloid. The parameters A and B are as follows:

$$A = 1/14340, \quad B = 1/9150$$

the dashed track is for corrected A and B with $A = 1/9150$, $B = 1/6100$ for the northern sector. The vortex data, obtained by averaging observed data is displayed in Table 7.

TABLE VII

$C_{x_0} = 5 \text{ kts}$	$x_1 = 1100 \text{ kms}$
$C_{y_0} = 2.5 \text{ kts}$	$y_1 = 800 \text{ kms}$
$r_1 = 600 \text{ kms}$	$\phi_1 = 13.5^\circ \text{ N}$
$a = 40 \text{ kms}$	$\omega_0 = 4 \text{ hr}^{-1}$

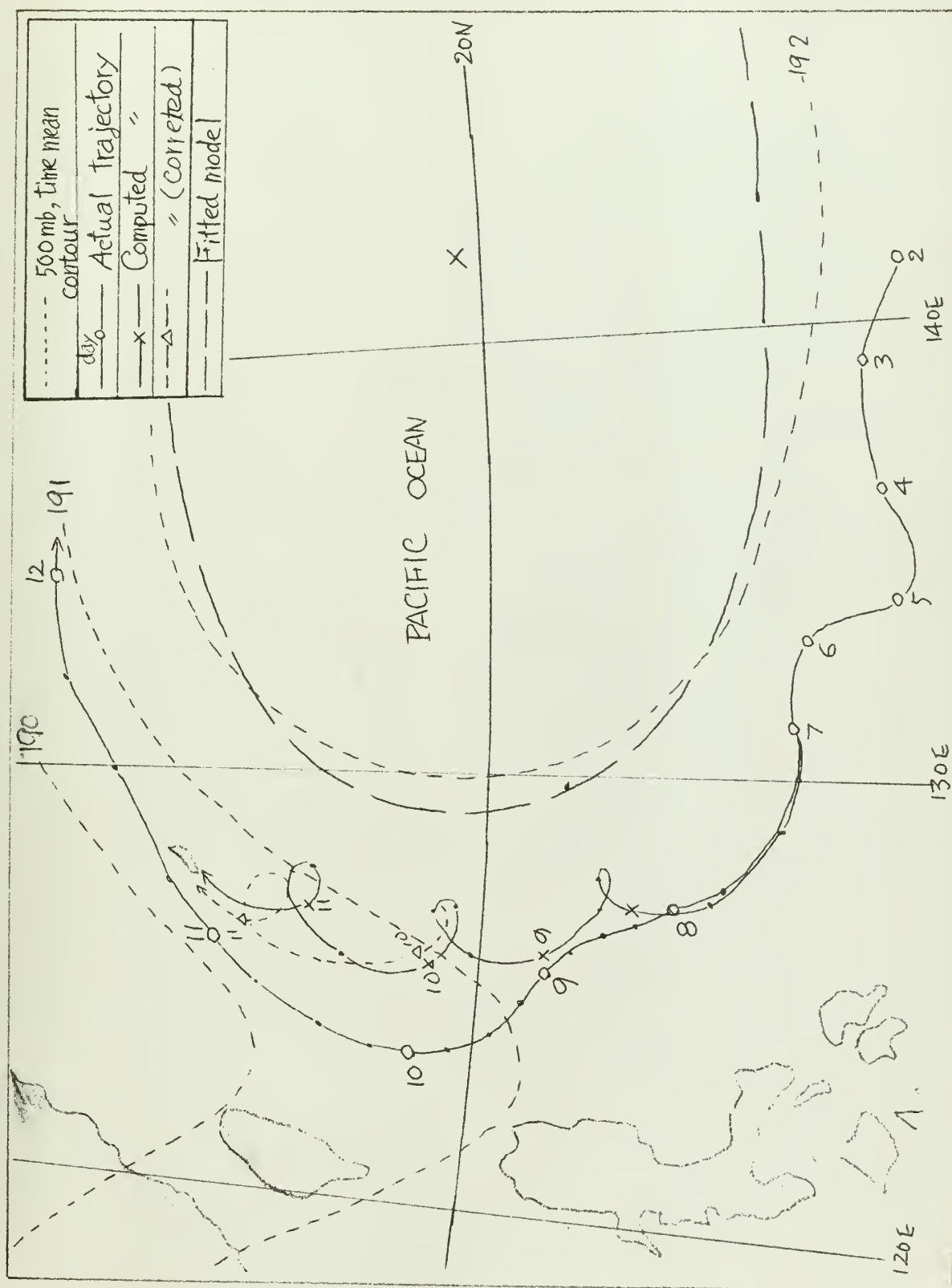


Figure 13 Typhoon "Clara" Nov. 1950

Figure 14 shows the same example but with a variable A and B. Assuming that A and B are linear functions of y only, A and B may be written as follows:

$$A \doteq A_0 + \left(\frac{\partial A}{\partial y}\right)y \quad , \quad B \doteq B_0 + \left(\frac{\partial B}{\partial y}\right)y$$

Here A_0 , B_0 are initial values for A and B. For this example the values are taken as:

$$A_0 = 1/14640$$

$$B_0 = 1/9150$$

$$\frac{\Delta A}{\Delta y} = 1/24400 / 1600 \text{ Kms}$$

$$\frac{\Delta B}{\Delta y} = 1/12200 / 1600 \text{ Kms}$$

Figure 15 also shows the same pattern, but represented by a hyperbolic paraboloid taking a similar variability for A and B as in the previous example. The values are taken as:

$$A_0 = 1/10460$$

$$B_0 = 1/6655$$

$$\frac{\Delta A}{\Delta y} = 1/18300 / 1600 \text{ Kms}$$

$$\frac{\Delta B}{\Delta y} = 1/10460 / 1600 \text{ Kms}$$

$$x_1 = -800 \text{ Kms}$$

$$y_1 = 550 \text{ kms}$$

The vortex, and other data are the same as in Table VII .

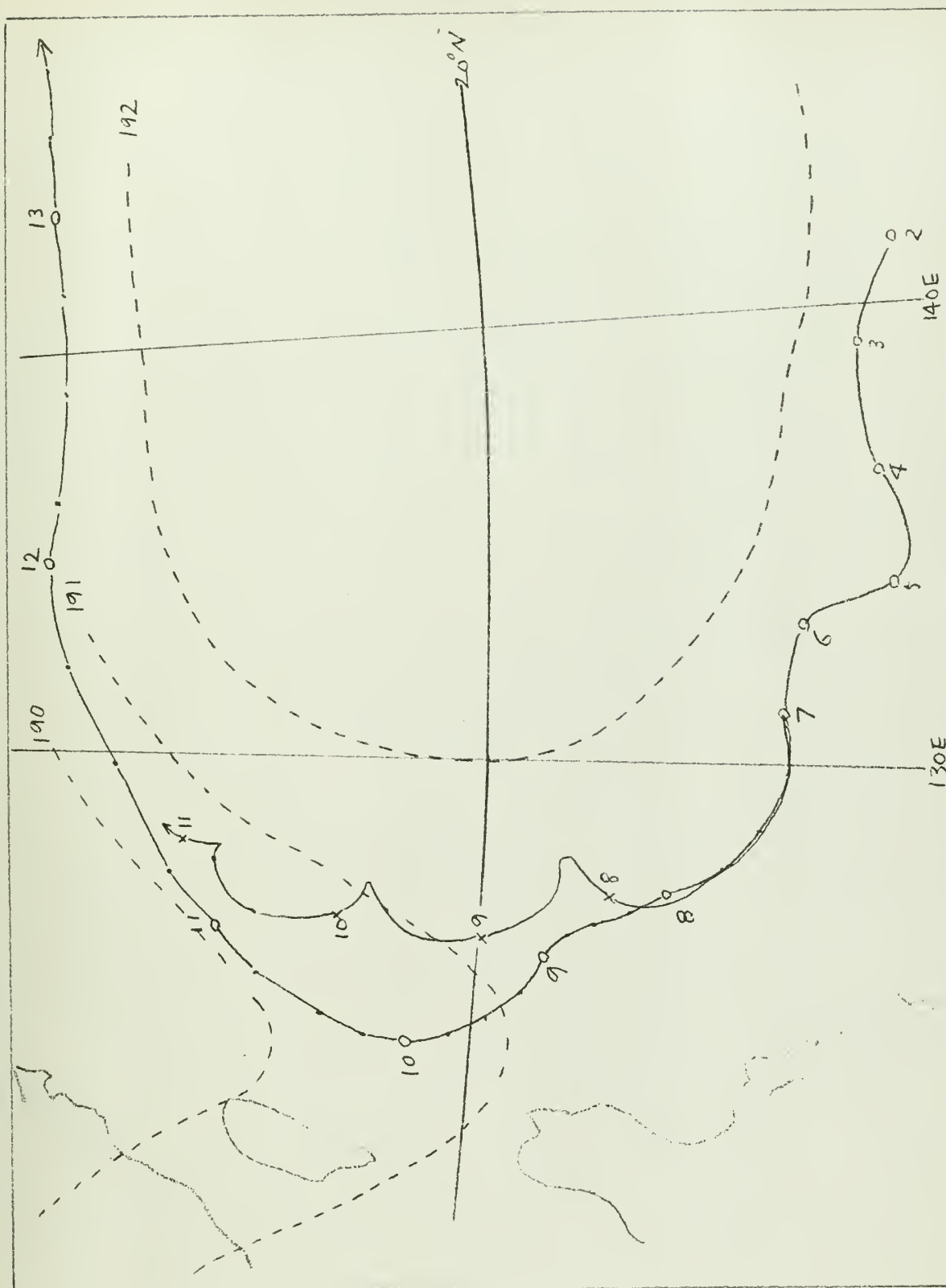


Figure 14

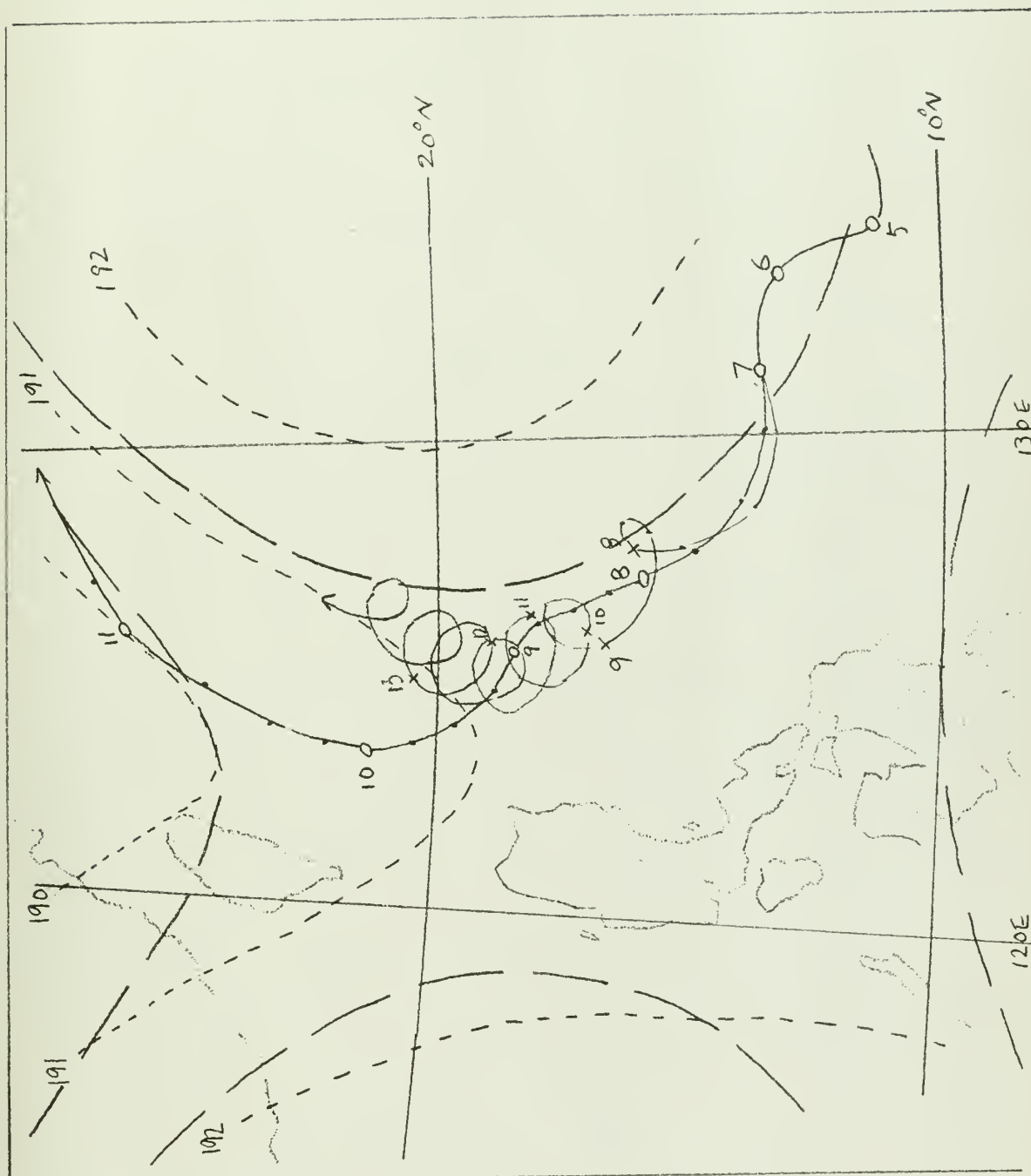


Figure 15

The second example is for the Typhoon "Jean" (Oct. 1956). The 5-day time-mean 500-mb map, representing the basic pressure pattern, is shown in Figure 16. The starting point is taken on 17th Oct. 1956, 0000 Japanese Local Time, (1500Z 16th). The mean 500-mb map seems to be the hyperbolic type. The parameters A and B are taken to be $A = 1/4440$, $B = 1/4070$, for track I, and $A = 1/4070$, $B = 1/3660$, for track II. The vortex model is shown in Table VIII.

TABLE VIII

$C_{x_0} = 10$ kts	$x_1 = 400$ kms
$C_{y_0} = 10$ kts	$y_1 = 600$ kms
$r_1 = 300$ kms	$\phi_0 = 18.5^\circ$ N
$a = 40$ kms	$\omega_0 = 2$ hr ⁻¹

The computed track follows the actual trajectory in direction, quite well; however the computed speeds are sometimes slow or fast. This results from an under- or over-estimate of the strength of the basic pressure gradient. Lack of time on the computer prevented further computations.

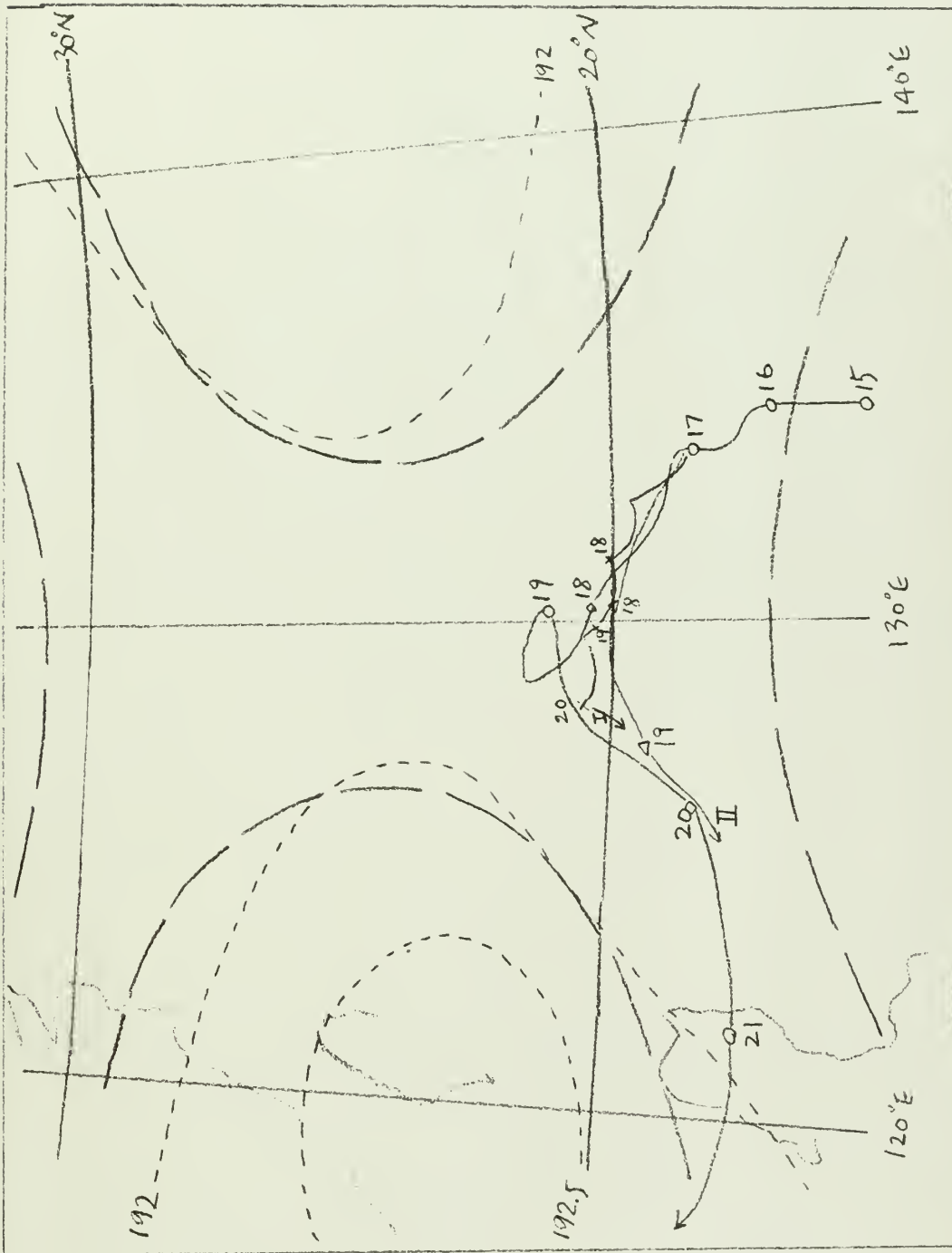


Figure 16 Typhoon "Jean", Oct 1956

5. Conclusions

Trajectories of tropical storms have been investigated and may be considered to consist of an oscillatory motion superimposed on a steered motion, with the latter generally dominating. Usually the amplitude of oscillation is small compared with the size of storms, hence it can not be recognized easily on daily maps. The oscillatory motion is superimposed on the steered motion and the result is a curve similar to a trochoid or cycloid. The period of the oscillation has been found theoretically to be $12/\sin\phi$ by many authors. In this study, the period was of the order of 1-2 days. The two examples of actual typhoons indicate that the results are applicable for a 3-5 day prediction of the trajectory of tropical storm, provided that the mean basic pressure field can be satisfactorily predicted.

BIBLIOGRAPHY

1. Abdullah, A. J., 1953; Dynamics of Hurricanes. New York University Met. papers, Vol 2, No 2.
2. Elliott, R. D., 1944; Note on advective pressure changes. Mo. Weather Rev. 72, pp 89.
3. Kasahara, A., 1957; The numerical prediction of hurricane movement with the barotropic model. J. Met. 14, 386-402.
4. Kuo Hsiao-Lan, 1950; The atmospheric vortices and general circulation. J. Met. 7, 247-258.
5. Murakami, T., Masuda, Y., and Arakawa, A.; On the distribution of vertical velocity and the numerical prediction of the movement of typhoon. Paper in Met. & Geoph. Vol. VII, 3.
6. Petterssen, S., 1945; Contribution to the theory of pressure variation. Quart. Journ. 71, 51-73.
7. Syono, S., 1951; On the motion of a vortex in a non-uniform pressure field. Papers in Met. & Geoph Vol II, 2.
8. Takeuchi, M., 1952; The motion of tropical cyclones in a non-uniform flow field. Papers in Met. & Geoph. Vol III, 4.
9. Yeh Tu-Chen, 1950; The motion of tropical storms under the influence of a superimposed southerly current. J. Met. 1, 105-118.

thesN24

Motion of the tropical storm.



3 2768 002 01753 5

DUDLEY KNOX LIBRARY